Collinear light modulation by surface acoustic waves in laterally structured semiconductors

Paulo V. Santos[a)]
Paul-Drude-Institut für Festkörperelektronik, Hausvogteiplatz 5–7, 10117 Berlin, Germany

(Received 19 September 2000; accepted for publication 6 February 2001)

The modulation of light beams by surface acoustic waves (SAW) in periodically modulated photonic materials is investigated. The periodic modulation allows for new scattering processes which can improve the efficiency of SAW-based modulators, as proposed by P. St. J. Russell [Phys. Rev. Lett. **56**, 596 (1986)]. In particular, scattering geometries with collinear propagation paths for the SAW and the light beam become possible using SAW wavelengths much larger than the light wavelength. We analyze the performance of such modulators based on semiconductor materials and examine the role of random fluctuations in structure dimensions on their operation. © *2001 American Institute of Physics.* [DOI: 10.1063/1.1359753]

I. INTRODUCTION

Materials with spatially modulated optical properties, such as photonic band gap crystals,[1–3] have received substantial attention during the last few years due to their ability to confine light beams within dimensions of the order of the light wavelength. In these materials, the light propagation properties can be tailored by controlling the structural dimensions and/or the composition profile. As a result, they have been envisaged as basic media for ultrasmall optical cavities as well as for integrated optical circuits.

Until now, most applications of photonic lattices have focused on passive optical elements like Bragg mirrors, light cavities, and waveguides. Active devices based on photonic lattices require the control of the structural dimension or of the materials' optical properties by an external signal. The modulation of the photonic lattice opens new fields of application for photonic lattices since it allows for dynamic control of the light flow. In a recent report, Busch and John[4] have proposed tunable photonic crystals consisting of liquid crystals encapsulated in a photonic lattice. The tunability in this case is achieved by modifying the optical properties of the liquid crystal through the application of an external electric field or by changing the temperature.[5,6]

An alternative approach for controlling light propagation in a structured medium is based on the utilization of a bulk or a surface acoustic wave. In particular, surface acoustic waves (SAWs[7–9]) can introduce a periodic modulation in the electronic properties of conventional crystals in the direction parallel to the surface with frequencies up to the gigahertz range. This periodic modulation constitutes the basis of operation of a whole class of acousto- and electro-optical devices,[10–12] such as optical spectrum analyzers, light modulators, and light switches. In a structured medium, the strain accompanying the acoustic wave will modulate not only the optical properties of the constituent materials but also their structural dimensions. In a piezoelectric crystal, the acoustic waves also possess a piezoelectric field which can affect the optical properties through the electro-optical mechanism.

The application of acoustic waves to modulate the optical properties of materials structured in one dimension was originally suggested by Russell,[13,14] who developed a coupled mode theory to account for the modulation process. In unstructured materials, light modulation by acoustic waves arises from Bragg diffraction of the light beam in the periodic refractive index grating created by the acoustic field. The momentum conservation for the diffraction process severely restricts the possible propagation directions of the light and of the SAW beams. The important aspect of laterally structured lattices resides in the modification of the momentum conservation rule for light diffraction by the acoustic wave.[13,14] As a result, new scattering geometries can be employed, which lead to substantial improvements in light modulation efficiency. In particular, scattering geometries with collinear propagation paths for the light and acoustic wave beams become possible even for acoustic waves with wavelengths much larger than the light wavelength. Recently, the feasibility of these concepts has been experimentally verified in fiber Bragg gratings modulated by acoustic waves.[15,16]

In this work, we will address light propagation in laterally structured semiconductor waveguides driven by SAWs. In particular, we will explore the unusual light propagation properties in the structured medium for applications in light modulators with collinear light and SAW propagation directions. The article is organized as follows: we start in Sec. II with a brief review of the principle of operation and of the limitations of conventional light modulation cells based on SAWs. The interaction between SAWs and light beams in structured materials is then analyzed: it is demonstrated that these structures can be employed in modulators with improved efficiency. As an example of the applicability of the new concepts, we present in Sec. III a simulation of light modulators based on semiconductor materials with a one-dimensional lateral modulation. The main conclusions are summarized in Sec. IV.

[a)]Electronic mail: santos@pdi-berlin.de

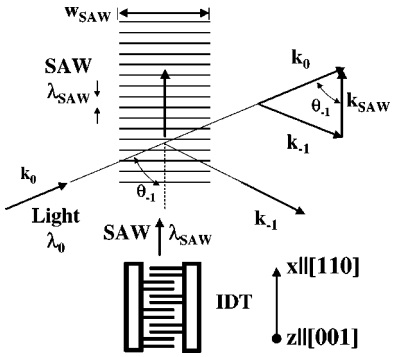

FIG. 1. Bragg diffraction of a light beam on a surface acoustic wave generated by an interdigital transducer (IDT).

II. LIGHT MODULATION BY SAWS

In this section the basic concepts involved in light modulation by a SAW are briefly reviewed. For that purpose, it will be considered that the light is modulated by a Rayleigh SAW propagating along the $x||[110]$ direction of the $z||[001]$ surface of a cubic semiconductor, as illustrated in Fig. 1. The acoustic displacement field **u** of a Rayleigh wave vanishes along $y||[1\bar{1}0]$ and decreases towards the substrate with a decay length comparable to the SAW wavelength λ_{SAW}. The displacement field can be expressed as $\mathbf{u}=[u_x(z),0,u_z(z)]\exp[\imath(k_{SAW}x-\omega_{SAW}t)]$, where $k_{SAW}=2\pi/\lambda_{SAW}$ and ω_{SAW} denote the SAW wave vector and frequency, respectively. The [110] propagation direction was chosen because in a piezoelectric zinc-blende crystal SAWs propagating along this direction can be electrically excited using interdigital transducers (IDTs) driven by an rf voltage. The concepts presented here, however, can be readily extended to other SAW types and to other propagation directions.

In order to model the interaction between the SAW and a light beam, we will neglect electro-optical effects and assume that the interaction is dominated by the acousto-optical mechanism, i.e., by the changes $\Delta\varepsilon$ in the dielectric function ε induced by the SAW strain. It will be further assumed that the light propagates in a waveguide close to the surface of the sample. The thickness of the waveguide and of its cladding layers are much smaller than λ_{SAW}. Under this approximation, the waveguide will not significantly affect the SAW fields, which will be approximately constant across the waveguide thickness.

The SAW reduces the symmetry of the cubic crystal. As a result, $\Delta\varepsilon$ becomes a tensor. In the basis $\{x,y,z\}$ defined above, this tensor can be expressed in terms of the photoelastic coefficients p_{ij} as[17]

$$\Delta\varepsilon=\varepsilon_0\begin{bmatrix}\frac{p_{11}+p_{12}+2p_{44}}{2}u_{xx}+p_{12}u_{zz} & 0 & 2p_{44}u_{xz}\\ 0 & \frac{p_{11}+p_{12}-2p_{44}}{2}u_{xx}+p_{12}u_{zz} & 0\\ 2p_{44}u_{xz} & 0 & p_{12}u_{xx}+p_{11}u_{zz}\end{bmatrix}e^{\imath[k_{SAW}x-\omega_{SAW}t]}, \quad (1)$$

where ε_0 is the dielectric function of the undisturbed crystal and u_{ij} denotes the amplitude of the strains generated by the SAW.

Equation (1) indicates that the light eigenstates consist of a mode polarized along y and of two elliptically polarized modes in the x-z plane. The ellipticity arises from the fact that, for a Rayleigh wave, the strain component u_{xz} is shifted by 90° with respect to u_{xx} and u_{zz}.[18,19] If we neglect the coupling between the x and z polarized modes introduced by the shear component u_{xz}, Eq. (1) corresponds to the dielectric tensor of a biaxial medium with main optical axis along x, y, and z. In this approximation, the relative change $\delta n_i/n_0$ in the refractive index along the main axis i $(i=x,y,z)$ is related to the diagonal tensor components of Eq. (1) by

$$\frac{\Delta n_i}{n_0}=\frac{1}{2}\frac{\Delta\varepsilon_{ii}}{\varepsilon_0}, \quad i=1,2,3, \quad (2)$$

where $n_0^2=\varepsilon_0$. Note that Eqs. (1) and (2) are only strictly valid if the thickness of the waveguide is much smaller than the SAW wavelength, so that the strains can be assumed constant across the width of the light beam. Otherwise, the depth dependence of the strain field may couple the y and the $x-z$ polarized modes.

The adimensional photoelastic coefficients p_{ij} in Eq. (1) are of the order of 10^{-1} for photon energies away from electronic resonances, while the strain amplitudes for electrically generated SAWs lie in the 10^{-4} range. As a result, the relative changes in the refractive index $\Delta n/n_0\sim10^{-4}$ are very small. In order to obtain high light modulation levels, the interaction path l_{SAW} between the SAW and the light beam must be sufficiently long to induce phase shifts of the light electric field comparable to π, i.e., $l_{SAW}>\lambda_0/(2\Delta n)\sim10^4\lambda_0$. To ensure constructive phase modulation over the long interaction path (or, equivalently, momentum conservation in the scattering process), SAW-based light modulators employ coherent Bragg reflection of the input light beam on the SAW wave fronts, as illustrated in Fig. 1. The SAW is generated by an interdigital transducer (IDT) deposited on the surface of a piezoelectric substrate. The Bragg reflection of the input light beam on the periodic SAW field leads to diffracted beams with a propagation direction (described by

the wave vector $\mathbf{k_p}$ for the pth order diffraction) and energies ($\hbar\omega_p$) that depend on the SAW wavelength λ_{SAW} and frequency ω_{SAW} according to

$$\mathbf{k}_{SAW}=\mathbf{k}_0-\mathbf{k}_p \quad \text{and} \quad \omega_{SAW}=\omega_0-\omega_p, \tag{3}$$

where ω_0 is the angular frequency of the incident light beam. Modulation of the intensity and of the propagation direction of the diffracted beams can then be achieved by changing, respectively, the intensity and the wavelength of the SAW.

As a consequence of Eq. (3), the angle θ_{-1} between the incident light beam and SAW beams for the first diffraction order becomes

$$\cos\theta_{-1}=\frac{1}{2n_0}\frac{\lambda_0}{\lambda_{SAW}}, \tag{4}$$

where λ_0 denotes the light wavelength (cf. Fig. 1). Equation (4) has important consequences for the operation of SAW-based light modulators in the visible and near-infrared range. These devices use SAWs with frequencies in the presently achievable range from 0.1 to 5 GHz, corresponding to wavelengths between one and a few micrometers. Since $\lambda_{SAW} \gg \lambda_0/n_0$, the angles θ_{-1} required for first order Bragg diffraction are normally close to 90°. The interaction length $l_{SAW}=d_{SAW}/\sin\theta_{-1}$, and thus the light modulation levels, become limited by the width w_{SAW} of the acoustic beam. The quasiperpendicular propagation paths of the SAW and light beams imply an inefficient use of the acoustic power since only a small portion of the SAW beam is useful for light modulation. In addition, the angle for Bragg reflection depends both on λ_{SAW} and λ_0. As a consequence, a change in the modulation frequency ω_{SAW} requires a corresponding change in the incident angle θ_{-1}.

The limitations mentioned above do not appear in a collinear interaction geometry where $\theta_{-1}=0$. The interaction path in this case can be made large, thus leading to higher modulation levels. The collinear interaction, however, requires $\lambda_{SAW}=\lambda_0/(2n_0)$, which for light in the near infrared range corresponds to exceedingly high SAW frequencies (in the tens of gigahertz range). An exception is provided by anisotropic Bragg reflection, where the diffraction process couples light beams of different polarizations.[10] The anisotropic diffraction requires that the two modes with different polarization possess collinear wave vectors differing by $\mathbf{k}_{SAW}$. In addition, the two light modes must interact with each other in the presence of the SAW field. Note that for cubic materials the last condition is not fulfilled for collinear propagation since, according to Eq. (1), the Rayleigh SAW does not couple the TE and TM modes.

As mentioned in the Introduction, the limitations can be overcome by employing a periodically structured light propagation medium.[13,14] In order to illustrate this concept, the one-dimensional structure illustrated in Fig. 2 will be considered. The periodically structured waveguide consists of alternating stripes of materials M_1 and M_2 with refractive indices n_1 and n_2, respectively. Light confinement in the waveguide is ensured by the cladding layer M_c deposited on the substrate M_s. The dispersion relation for light modes propagating along x is shown in Fig. 3. In contrast to the linear $\hbar\omega_0$ versus k dispersion of unstructured materials

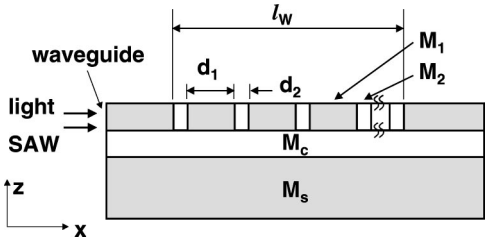

FIG. 2. Structure of a Bragg reflection cell using a periodically structured medium composed of materials M_1 and M_2. M_c and M_s denote the cladding layer and substrate, respectively. l_W denotes the length of the modulated region of the waveguide.

(dashed line in Fig. 3), the light dispersion of the structured medium folds into a mini-Brillouin zone of dimension $2\pi/d$, where $d=d_1+d_2$ is the modulation period. In addition, the dispersion shows gaps in the center and at the boundary of the mini-Brillouin zone, corresponding to energy ranges where no propagating light mode is allowed due to constructive reflection on the lateral interfaces. For normal Bragg diffraction on a SAW, indicated by A in Fig. 3, the momentum conservation rule stated in Eq. (3) applies and the SAW wave vector is connected to the light wave vector by $k_{SAW}=2k_0$. Here, it was assumed that $|k_{-1}|\sim|k_0|$, which is an excellent approximation in view of the large difference between the photon and acoustic wave energy quanta.

The important aspect of the dispersion folding is that it allows for umklapp scattering processes such as the ones indicated by B and C in Fig. 3. For these processes, the momentum conservation in Eq. (3) applies up to a grating wave vector $k_G=2\pi/d$, i.e.,

$$k_{SAW}=mk_G\pm 2k_0, \tag{5}$$

where m is an integer ($m=0$ corresponds to normal Bragg reflection). The umklapp process illustrated by B and C in Fig. 3 corresponds to $m=+1$ and $m=-1$, respectively. Equation (5) shows that by a suitable choice of the artificial periodicity it becomes possible to have collinear Bragg reflection with SAW wave vectors considerably smaller than the light wave vector. For applications, this means that SAW frequencies in the few GHz range can be used to drive collinear light modulators.[15]

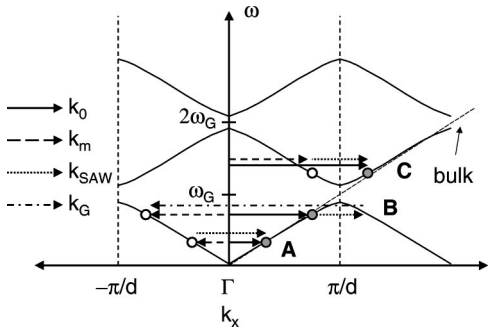

FIG. 3. Light dispersion in a periodically structured material displaying normal (A) and umklapp scattering processes (B and C). The arrows display the wave vectors of the incident light (k_0, solid arrow), of the diffracted light (k_m, dashed arrow), of the SAW (k_{SAW}, dotted arrow), and the grating wave vector $k_G=2\pi/d$(dash-dotted arrow).

Umklapp Bragg reflection processes similar to the one discussed above have been investigated in the context of folded acoustic phonons in semiconductor superlattices.[20–23] In these investigations, the umklapp scattering of photons by thermal acoustic phonons leads to the observation of additional lines in the Raman spectrum. Although a physical mechanism similar to that illustrated in Fig. 3 is operative, there is an important difference to the case considered here. In the folded phonon studies the artificial periodicity d is normally much smaller than the light wavelength. As a result, it mainly affects the propagation properties of thermal acoustic phonons with a wavelength comparable to d. In the scattering processes investigated here, however, the artificial periodicity is chosen to be comparable to the light wavelength, so that it affects primordially the light propagation. The wavelength of the acoustic wave is supposed to be much larger than the modulation period, so that its propagation properties will not be substantially affected by the periodicity.

Although the discussion above has been based on materials with a one-dimensional composition modulation, the same concepts apply to SAW-induced light modulation in two- and three-dimensional photonic structures. The SAW in these cases can be used to control not only the intensity but also the propagation direction of light in the photonic medium. The simplicity of the one-dimensional structures, however, allows for a direct physical insight into the modulation process and considerably simplifies the calculation of the modulation intensity, as will be demonstrated in the next section.

III. NUMERICAL SIMULATIONS

The feasibility of collinear Bragg reflection using acoustic waves with wavelengths much larger than the light wavelength has been demonstrated experimentally in fiber Bragg gratings by Liu and coworkers.[15,16] In order to demonstrate the applicability of the same concepts for semiconductor waveguides driven by a SAW, we will consider a one-dimensional grating of the type illustrated in Fig. 2 based on the GaAs/(Al,Ga)As material system. The waveguide consists of GaAs stripes (material M_1) with air spacers (material M_2) deposited on GaAs substrate (M_s) covered by an AlAs cladding layer (material M_c). In the long light wavelength limit, the effective refractive index of the waveguide becomes $n_{\text{eff}}=(n_{\text{GaAs}}d_{\text{GaAs}}+d_{\text{air}})/(d_{\text{GaAs}}+d_{\text{air}})$. In order to ensure light confinement in the waveguide, we used a width ratio $\alpha=d_{\text{GaAs}}/d=0.85$, which yields $n_{\text{eff}}=2.97>n_{\text{AlAs}}=2.88$ for $\hbar\omega_0=1.3\mu$m. A period $d=167$ nm was chosen so as to yield a gap in the dispersion at a light wavelength of 1.0 μm. Note that lower values of α can be used if the cladding layer is also structured.

The optical properties of the waveguide are modulated by a SAW with a wavelength $\lambda_{\text{SAW}}=1\mu$m propagating along the x direction. The lateral structuring will also modify the propagation properties of the SAW.[24,25] In the following analysis, such effects will be neglected based on the fact that the SAW wavelengths used here are considerably larger than the structural dimensions. More detailed calculations will be required to check the validity of this approximation.[26–28] The changes in the refractive index induced by the SAW were determined based on the same assumptions made in connection with Eqs. (1) and (2). The SAW strain fields were calculated following the procedure described in Ref. 18,[19] the photoelastic coefficients for GaAs, necessary for the determination of the refractive index modulation, were extracted from Ref. 29.

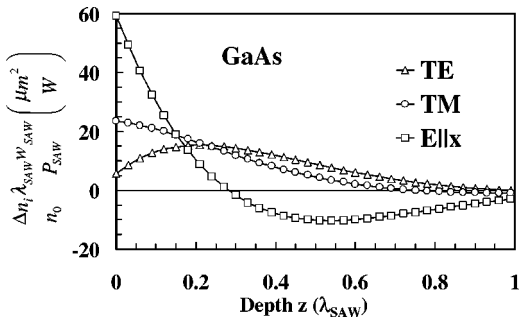

FIG. 4. Depth dependence of the refractive index modulation $\Delta n_i/n_0$ by a SAW in GaAs for TE (electric field E parallel to $y=[1\bar{1}0]$ corresponding to $i=2$) and TM ($E||z=[001]$, $i=3$) polarizations, and for $E||x=[110]$ ($i=1$).

The depth dependence of the SAW-induced refractive index modulation $\Delta n_i/n_0$ for GaAs, normalized to the effective power density $P_{\text{SAW}}/(\lambda_{\text{SAW}}w_{\text{SAW}})$ of the SAW beam, is displayed in Fig. 4. In the last expression, P_{SAW} denotes the power of the SAW beam. The triangles and circles display the refractive index modulation for the TE and TM light modes, which are the relevant ones for collinear propagation of the SAW and light beams. For comparison we also include the modulation of the refractive index for light polarized along the x direction (squares), which is relevant for quasiorthogonal scattering geometries with incident light polarized along x.

Light propagation within the one-dimensional waveguide of Fig. 2 can be calculated using the coupled-mode approach introduced by Russell.[13,14,15,30] Here, however, we opted for a numerical transfer matrix approach since it (i) allows for a direct calculation of the light transmission and reflection coefficients in finite waveguides and (ii) can easily take into account disorder effects. For that purpose, each GaAs stripe centered at the position $\bar{x}$ was assumed to have a constant refractive index $n_{\text{TE(TM)}}(\bar{x})=n_{\text{GaAs}}(1+\Delta n_{\text{TE(TM)}}/n_{\text{GaAs}}\cos[k_{\text{SAW}}\bar{x}-\omega_{\text{SAW}}t])$. This assumption is justified as long as the widths of the stripes remain much smaller than λ_{SAW}. The time dependence of the refractive index modulation leads to a coupling of light modes with angular frequencies ω_m Doppler shifted with respect to the frequency ω_0 of the incident beam. As a result, the light modes within each stripe can be expressed as a superposition of plane waves with amplitudes A_m and frequencies $\omega_m=\omega_0+m\omega_{\text{SAW}}$, where $m=0,\pm1,\pm2,\ldots$. In the transfer matrix approach, the amplitudes A_m in adjacent slabs are related to each other by a matrix (the transfer matrix) describing the electromagnetic boundary conditions at the interface between the stripes.[8] The dimension of the matrices thus becomes $(2m+1)\times(2m+1)$. The amplitude and phase

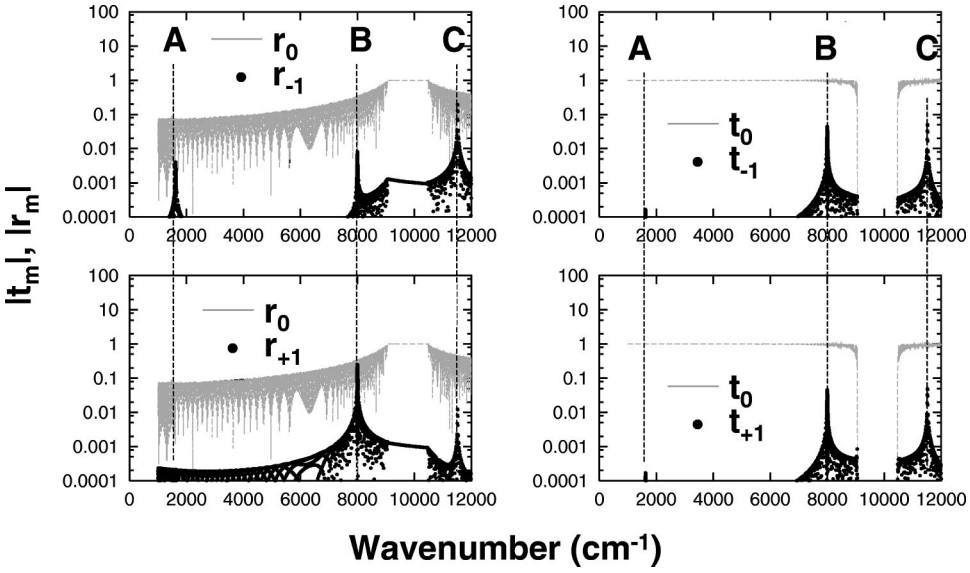

FIG. 5. Wave number dependence of the reflection ($|r_m|$, left panels) and transmission ($|t_m|$, right panels) coefficients for collinear Bragg reflection on a SAW. The apparent scattering in the data points arise from Fabry–Perot interference fringes in the length l_W of the modulated waveguide (see Fig. 2).

of the modes will be described in terms of complex reflection and transmission coefficients r_m and t_m, respectively.

For the numerical calculations we used for the GaAs stripes $\Delta n/n_0 = 7\times 10^{-4}$, which corresponds to the refractive index modulation for both TE and TM polarizations at a depth of $0.2\lambda_{\mathrm{SAW}}$ from the surface induced by a SAW with a beam width $w_{\mathrm{SAW}} = 20\mu$m and $P_{\mathrm{SAW}} = 0.5$ mW ($\lambda_{\mathrm{SAW}} = 1\mu$m) on an unstructured GaAs substrate. Only modes with $|m| \leqslant 1$ were considered. The results, therefore, apply strictly only for amplitudes $|r_{\pm 1}| \ll 1$ and $|t_{\pm 1}| \ll 1$. The procedure, however, can be easily extended to include higher m values.

The spectral dependence of $|r_m|$ and $|t_m|$ ($m = -1,0,1$) for a structured waveguide with length $l_W = 100\ \lambda_{\mathrm{SAW}}$ terminated by GaAs regions is displayed in Fig. 5. The oscillations (indicated by the shaded area and by the apparent scattering in the data points) arise from Fabry–Perot interference fringes in the total length l_W of the modulated waveguide. The fringes can be eliminated by introducing antireflecting structures at the left and right ends of the modulated region. The first gap in the light dispersion, which is indicated as ω_G in Fig. 3, appears as a minimum (maximum) in $|t_0|$ ($|r_0|$) centered at 10 000 cm^{-1}. The maximum in $|r_{\pm 1}|$ at 1800 cm^{-1} corresponds to the normal scattering process indicated by *A* in Fig. 3. The umklapp processes *B* and *C* give rise to the peaks in $|r_{\pm 1}|$ at 8000 cm^{-1} and 11 500 cm^{-1}.

The dynamic scattering processes lead to maxima at the reflection ($|r_m|$, $m = \pm 1$) and in the transmission coefficients ($|t_m|$) in the presence of a SAW. According to Eq. (5), the energy of the maxima is controlled by the SAW frequency. The SAW driven modulated waveguide thus becomes a tunable light filter with center frequency ω controlled by ω_{SAW} according to

$$\omega = \omega_G \pm \frac{c}{n_{\mathrm{eff}} v_{\mathrm{SAW}}} \omega_{\mathrm{SAW}}, \tag{6}$$

where c denotes the light speed and v_{SAW} the SAW propagation velocity. The positive and negative signs apply to processes *C* and *B*, respectively (cf. Fig. 3). Equation (6) neglects the flattening of the dispersion near the edges of the Brillouin zone. An example of tunability is illustrated in the calculation results displayed in Fig. 6. By varying the SAW wavelength by 10% the peak reflection frequency of $|r_1|$ can be shifted over a wide range. The wide tunability range arises from the large ratio $c/(n_{\mathrm{eff}} v_{\mathrm{SAW}})$ between the light and the SAW propagation velocities in the medium, which compensates for the small ratio between the SAW and light frequencies $\omega_{\mathrm{SAW}}/\omega_0$. Note that for an ideal (i.e., lossless) waveguide, the width of the reflection peaks becomes determined by the total length of the interaction region (of 100 μm in Fig. 6).

The relative intensities of the $|r_{-1}|$ and $|r_{+1}|$ reflection (and of the $|t_{-1}|$ and $|t_{+1}|$ transmission) coefficients depend on two main factors. The first, and the more important, is energy conservation during the scattering of a photon propa-

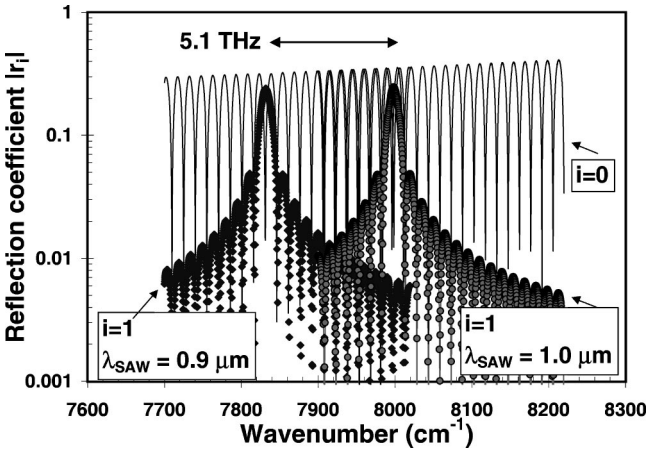

FIG. 6. Absolute value of the complex reflection coefficient of the structure in Fig. 2 for the unshifted ($|r_0|$, solid line) and for the up-shifted ($|r_1|$, symbols) beams under modulation by a SAW with wavelengths of $\lambda_{\mathrm{SAW}} = 1.0\ \mu$m (diamonds) and $\lambda_{\mathrm{SAW}} = 0.9\ \mu$m (circles). The oscillations in the spectra arise from Fabry–Perot interference fringes in the total length $l_W = 100\ \mu$m of the structured waveguide.

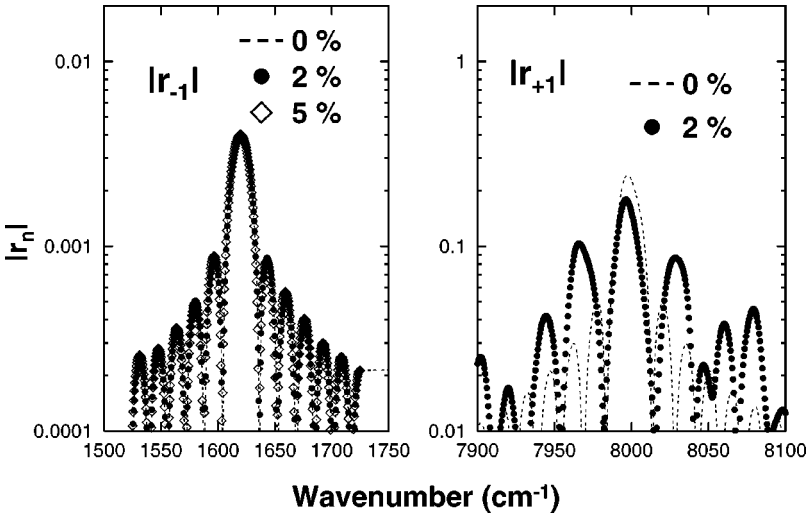

FIG. 7. Wave number dependence of the reflection ($|r_m|$) coefficients of the first (left panel) and second (right panel) Bragg reflection peaks in Fig. 5 including the effect of random fluctuation of the lateral sizes d_1 and d_2 in Fig. 2. The disorder is quantified in terms of the standard deviation in the lateral sizes of 0% (dashed line), 2% (dots), and 5% (diamonds).

gating along the $+\hat{\mathbf{x}}$ direction (indicated by closed circles in Fig. 3) into a photon propagating in the opposite direction (open circles) by a SAW mode with $\mathbf{k}_{\mathrm{SAW}}=k_{\mathrm{SAW}}\hat{\mathbf{x}}$. For processes *A* and *C*, the only possible Bragg-reflection process corresponds to the emission of a SAW quantum, leading to a redshifted scattered photon with energy $\hbar\omega_0-\hbar\omega_{\mathrm{SAW}}$.[31] As a result, in the absence of multiple scattering events the only nonvanishing reflection coefficient should be $|r_{-1}|$. For process *B*, however, a SAW quantum is emitted and only $|r_{+1}|\neq 0$.

The second factor controlling the $|r_m|$'s (and $|t_m|$'s) is light reflection at the boundaries of the modulated region, which also gives rise to the Fabry–Perot interference fringes observed in Figs. 5–7. As a consequence of reflection, the light field in the modulated region becomes a superposition of eigenmodes of the periodically modulated lattice (Floquet–Bloch waves[13,28]) with counter propagating wave vectors $+k_m\hat{\mathbf{x}}$ and $-k_m\hat{\mathbf{x}}$ (this is valid even in the absence of a SAW). For low photon energies (as for process *A*), the light wavelength is significantly larger than the modulation period. The structured region can then be considered as a homogeneous medium with an effective refractive index n_{eff}. In this case, the reflection coefficient $r_0=(n_{\mathrm{eff}}-1)/(n_{\mathrm{eff}}+1)$ is relatively small. It becomes a good approximation to assume that only the $+k_m\hat{\mathbf{x}}$ is excited, so that $|r_{-1}|\gg|r_{+1}|,|t_{\pm 1}|$. The structural modulation becomes important as the photon energy approaches the gaps in the light dispersion. Close to the gap, reflection at the boundaries of the modulated region increases significantly (see r_0 in Fig. 5) and the relative amplitudes of the $+k_m\hat{\mathbf{x}}$ and $-k_m\hat{\mathbf{x}}$ components become comparable. The interaction of these modes with the SAW leads to the nonvanishing coefficients r_m and t_m $(m=\pm 1)$ displayed in Fig. 5 for processes *B* and *C*.

The nonvanishing transmission under Bragg reflection conditions indicates that the structure of Fig. 2 can be used as a light modulator not only in the reflection geometry but also as a high resolution tunable filter in the transmission geometry. The transmitted signal (detected, e.g., by a photodiode) is proportional to $I_d=|t_0+t_{+1}+t_{-1}|^2$. This signal has a component at the SAW frequency ω_{SAW} proportional to $|t_{\pm 1}|$, which can be easily separated by synchronous (i.e., phase sensitive) detection at the SAW frequency. The frequency selectivity achieved by synchronous detection can be used to replace the spatial selectivity resulting from changes in the Bragg reflection angle, which is the principle of operation of spectrum analyzers based on noncollinear SAW modulators. Note that the detected intensity in the former case is proportional to $|t_{\pm 1}|$, whereas for noncollinear modulators the detected intensities are proportional to the square $(|r_{\pm 1}|^2)$ of the diffraction amplitudes. For this reason, the transmission and reflection coefficients were plotted in Fig. 5 as $|t_m|$ and $|r_m|$, respectively, instead of intensities $|t_m|^2$ and $|r_m|^2$.

An important aspect connected to light modulators and filters based on umklapp processes concerns the role of imperfection in the periodic structure on their performance. In particular, random fluctuation in the dimensions d_1 and d_2 of the lateral structures of Fig. 2 are expected to introduce an effective broadening Δk in the $\hbar\omega$ versus k dispersion curve of Fig. 3. As a consequence, the SAW couples light modes with a range of k vectors, thus leading to a deterioration of frequency selectivity.

The effects of the random fluctuations are illustrated in Fig. 7. The left (right) panel displays the reflection coefficient $|r_{-1}|$ ($|r_{+1}|$) in the energy range close to the first (second) Bragg reflection peaks at 1625 cm^{-1} (8000 cm^{-1}) in Fig. 5 for different levels of disorder. As for Fig. 5, the oscillations in Fig. 7 are due to Fabry–Perot interferences in the length l_W of the modulated waveguide. The disorder is quantified in terms of the standard deviation σ in the lateral dimensions d_1 and d_2. For the normal Bragg reflection peak at 1625 cm^{-1} (left panel in Fig. 7) the reflection coefficient is insensitive to the disorder up to high disorder levels ($\sigma>5\%$). The insensitivity results from the fact that the long light wavelength averages the optical properties over many periods *d*. For the umklapp scattering at 8000 cm^{-1} (right panel) relatively small levels of disorder broaden significantly the reflection peak. In contrast to the previous case, the wavelength of the light beam is now comparable to *d* and thus very sensitive to small length fluctuations. These results

demonstrate that high performance light modulators based on structured materials require a high degree of control of the dimensions of the lateral structures. Note that since we assumed that both d_1 and d_2 vary with disorder, the fluctuations also affect the modulation period. The results of Fig. 7 may thus overestimate disorder effects in structures produced by lithographic methods, where the fluctuations are expected to affect only the relative dimension of layers within one period, but not the period itself.

IV. CONCLUSIONS

We have investigated light modulation by a SAW in periodically structured medium. The periodic modulation allows for umklapp scattering, which can be employed for new geometries of SAW-based light modulators with improved modulation efficiencies. In particular, collinear scattering geometries can be designed using SAW with wavelengths considerably larger than the light wavelength. We presented calculations of the modulation efficiency of these structures and analyzed the effects of fluctuation in structural dimensions on their performance.

The concepts presented here are not restricted to composition modulation in one dimension. They can be extended to structures with two- and three-dimensional spatial modulation of the type employed in photonic band gap materials. Finally, although the discussion has been based on elasto-optical modulation by SAWs, the same concept applies for other modulation mechanisms as such the electro-optical and magneto-optical interactions.

ACKNOWLEDGMENTS

We gratefully acknowledge G. Jungk, H. Grahn, and M. Giehler for comments and for a critical reading of the manuscript.

[1] E. Yablonovitch, Phys. Rev. Lett. **58**, 2059 (1987).
[2] S. John, Phys. Rev. Lett. **58**, 2486 (1987).
[3] J. D. Joannopoulos, R. D. Meade, and J. N. Winn, *Photonic Crystals: Molding the Flow of Light* (Princeton University, Princeton, NJ, 1995).
[4] K. Busch and S. John, Phys. Rev. Lett. **83**, 967 (1999).
[5] K. Yoshino, Y. Shimoda, Y. Kawagishi, K. Nakayama, and M. Ozaki, Appl. Phys. Lett. **75**, 932 (1999).
[6] S. W. Leonard, J. P. Mondia, H. M. van Driel, O. Toader, S. John, K. Busch, A. Birner, U. Gösele, and V. Lehmann, Phys. Rev. B **61**, 2389 (2000).
[7] A. A. Maradudin, in *Modern Problems in Surface Physics: Proceedings of the First International School on Condensed Matter Physics* (Publishing House of the Bulgarian Academy of Science, Sofia, 1981), p. 11.
[8] B. A. Auld, *Acoustic Fields and Waves in Solids* (Robert E. Krieger, Inc, Malabar, FL, 1990).
[9] A. A. Oline, *Acoustic Surface Waves* (Springer, Berlin, 1994).
[10] A. Korpel, *Acousto-Optics* (Marcel Dekker, New York, 1997).
[11] C. S. Tsai, *Guided-Wave Acousto-Optics* (Springer, Berlin, 1990).
[12] C. S. Tsai, B. Sun, and A. Kar-Roy, Appl. Phys. Lett. **70**, 3185 (1997).
[13] P. St. J. Russell, Phys. Rev. Lett. **56**, 596 (1986).
[14] P. St. J. Russell, J. Appl. Phys. **59**, 3344 (1986).
[15] W. L. Liu, P. S. J. Russell, and L. Dong, Opt. Lett. **22**, 1515 (1997).
[16] W. L. Liu, P. S. J. Russell, D. O. Culverhouse, and R. Reekie, in *Conference on Lasers and Electro-Optics, Vol. 9 of 1996 OSA Technical Digest Series* (Optical Society of America, Washington, DC, 1996), p. 243.
[17] J. F. Nye, *Physical Properties of Crystals* (Oxford University, London, 1964).
[18] S. Simon, Phys. Rev. B **54**, 13878 (1996).
[19] The numeric value of the normalization factor H in Eq. (37) of Ref. 18 is incorrect. The correct value for GaAs is $H=1.067\times10^{11}$ N/m^2.
[20] C. Colvard, R. Merlin, M. V. Klein, and A. C. Gossard, Phys. Rev. Lett. **45**, 298 (1980).
[21] J. Sapriel, J. C. Michel, J. C. Toledano, and R. Vacher, J. Phys. C **45**, 139 (1984).
[22] P. V. Santos, M. Hundhausen, and L. Ley, Phys. Rev. B **33**, 1516 (1986).
[23] B. Jusserand, F. Alexandre, J. Dubard, and D. Paquet, Phys. Rev. B **33**, 2897 (1986).
[24] Y. Tanaka and S. Tamura, Phys. Rev. B **58**, 7958 (1998).
[25] T. Aono and S. Tamura, Phys. Rev. B **58**, 4838 (1998).
[26] The existence of surface acoustic waves in laterally structured media has been demonstrated both theoretically (see, for instance, Refs. 24 and 25) and experimentally (in Refs. 29 and 30).
[27] M. Torres, F. R. Montero de Espinosa, D. García-Pablos, and N. García, Phys. Rev. Lett. **82**, 3054 (1999).
[28] R. E. Vines, J. P. Wolfe, and A. V. Every, Phys. Rev. B **60**, 11871 (1999).
[29] *Landolt-Börnstein Tables Vol. 11*, edited by K. H. Hellwege (Springer-Verlag, Heidelberg, 1979).
[30] P. St. J. Russell, J. Mod. Opt. **38**, 1599 (1991).
[31] We neglect in this approximation the weak scattering processes involving thermal elastic waves (such as those treated in normal Brillouin scattering) based on the fact that their concentration is significantly smaller than those generated by the acoustic transducers.